Journal of Materials Chemistry C

ROYAL SOCIETY OF CHEMISTRY

PAPER

View Article Online
View Journal | View Issue

Cite this: J. Mater. Chem. C, 2025, 13, 23178

Nanoscale $Y_2SrZnO_5:Eu^{3+}$ luminescent inks: enhancing security and stability *via* triple excitation for advanced anti-counterfeiting measures

Payal P. Pradhan,[a] Tejaswi Jella,[b] M. Rakshita,[a] Aachal A. Sharma,[a] K. A. K. Durga Prasad[a] and D. Haranath *[a]

Received 23rd July 2025,
Accepted 9th October 2025

DOI: 10.1039/d5tc02801a

rsc.li/materials-c

Counterfeiting of classified documents and currency demands innovative materials to enhance their security. Here, we report a novel Eu^{3+}-doped Y_2SrZnO_5 (YSZO) nanopowder, synthesized *via* an optimized sol–gel combustion method, and its application as a stable, luminescent ink. This oxide-based phosphor exhibits exceptional photostability under 254 nm UV light, thermal resilience up to 120 °C, and resistance to solvents and humidity, making it a robust anticounterfeiting candidate. YSZO:Eu^{3+} displays intense red emission (550–750 nm) from $^5D_0 \rightarrow {}^7F_J$ (J = 0–3) transitions, achieving 99.8% color purity. Security labels printed with this ink remain invisible under daylight but reveal encrypted patterns under UV (254 nm), near-UV (393 nm), and blue (465 nm) light. Its multi-environment stability ensures durable luminescence, critical for tamper-proof authentication. Unlike traditional inks reliant on toxic solvents, this non-toxic YSZO:Eu^{3+} system offers a sustainable alternative with high contrast and selectivity. These properties position Eu^{3+}-doped YSZO as a breakthrough in materials chemistry, enabling reliable, counterfeit-resistant features for secure documents and currency.

1. Introduction

Counterfeiting, a global scourge impacting economies and safety, fuels illicit replication of currency, documents, and goods, with trade values soaring to USD 960 billion by 2015. According to estimates from the Organisation for Economic Cooperation and Development (OECD), the amount of money traded in counterfeit goods amounted to $250 billion in 2007 or 1.95% of the global trade.[1–3] A variety of technologies are used for anti-counterfeiting strategies: (i) digital methods (hashing fingerprinting, digital watermarks, and digital rights management systems) are used to embed and identify information; (ii) chemical and physical methods (chemical encoding, laser surface analysis, tracers, and surface fingerprint) are used to authenticate without concurrent distinctive product identification;[4–6] (iii) mechanical methods (anti-alteration devices, labels, and security films) are used to develop anti-falsify barriers and carry out basic authentication to protect and track the intellectual property content of computers, electronic devices, and digital files, (iv) electronic methods (seals, RFID, NFC, contact chips, and magnetic strips) are used to enable remote object recognition;[7] and (v) optical patterns (security inks, watermarks, encrypted images, and optical strips) are used to verify instead of identifying specific products.[8–10] Out of all the methods discussed above, the most intriguing and popular security feature is optical pattern. It enables visual inspection through straightforward verification processes, which frequently permit a visual inspection, or *via* inexpensive, basic devices. Effective countermeasures require nanoscale solutions that use unclonable, stable, and easily authenticated materials that are resilient to manipulation.[11]

In this regard, there is a constant need for luminescent materials with excellent properties in security inks for anti-counterfeiting applications. Currently, a wide range of compounds are utilized as fluorescent dyes in security printing inks. These materials include organic small molecules, rare-earth ions,[12–14] and carbon dots[15,16] that react to environmental stimuli including light, pressure, heat, solvent vapour, or chemicals. Rare earth (RE)-doped fluorescent materials that can be applied to print documents have been created to boost anti-counterfeit measures and prevent the threat of duplication and security breaches.[12,17–19]

Rare earth (RE)-doped nanopowders, distinguished by their narrowband emission, substantial Stokes shifts, and

[a] Luminescent Materials and Devices (LMD) Group, Department of Physics, National Institute of Technology Warangal, Hanumakonda 506004, Telangana, India. E-mail: haranath@nitw.ac.in; Fax: +91 870 245 9547; Tel: +91 995 810 1115
[b] Department of Chemistry, National Institute of Technology Warangal, Hanumakonda 506004, Telangana, India

exceptional luminescence, are transforming anticounterfeiting technologies. Compared to sulfide and fluoride hosts, which suffer from instability and toxicity, oxide-based hosts exhibit superior chemical durability, physical stability, and optical performance at the nanoscale.[20,21] Nevertheless, the development of non-toxic, high-efficiency nanoinks continues to pose a significant challenge in the face of increasingly sophisticated counterfeiting techniques.

Herein, we unveil Y_2SrZnO_5 (YSZO, ARE_2BO_5; A = Sr, RE = rare-earth, B = Zn) nanopowders, engineered *via* an optimized sol–gel combustion method. Doped with Eu^{3+}, YSZO exhibits triple-excitable luminescence (254 nm, 393 nm, 465 nm), intense red emission, and unmatched stability against light, heat, solvents, and humidity. Triple-excitation luminescent materials represent a pivotal advancement in security inks for anticounterfeiting applications. Unlike single- or dual-excitation systems, these materials enable multi-channel authentication through independent verification under ultraviolet (UV), near-UV, and blue-light excitation. This multifaceted optical response significantly reduces the potential for replication by counterfeiters. The consistent red emission across three distinct excitation wavelengths ensures a robust and unassailable signal, facilitating versatile detection with portable lamps or light emitting diode (LED) sources spanning multiple spectral regions. This unique triple excitation–emission behavior markedly enhances the ink's security, adaptability, and reliability, establishing it as an ideal solution for thwarting counterfeiting.

Unlike traditional inks reliant on hazardous solvents (*e.g.*, cadmium sulfide, cadmium selenide, and hexane), these non-toxic nanopowders enable sustainable, high-contrast security features. Stability encompasses the ink's resilience against the passage of time, environmental stressors, and adversarial manipulation. Applied as inks, they encrypt documents and currency, visible only under specific wavelengths, fortifying nanoscale defenses against forgery. This work heralds a leap in nanotechnology, merging stability and luminescence to combat counterfeiting at the molecular level.

2. Experimental

2.1. Materials and synthesis

A series of Eu^{3+}-doped Y_2SrZnO_5 (YSZO:xEu^{3+}) nanopowders (x = 0.01–0.3 mol) was synthesized *via* a self-igniting sol–gel combustion method, optimized for high-yield production of luminescent nanomaterials.[22] High-purity precursors Y_2O_3, $SrCO_3$, ZnO, and Eu_2O_3 (Sigma-Aldrich, ≥99.9%) were combined with citric acid ($C_6H_8O_7$, ≥99%) as a fuel, leveraging its role in morphology control.[23] Stoichiometric amounts of the oxides were dissolved in concentrated nitric acid (HNO_3) to form metal nitrates, followed by the addition of citric acid in a 4 : 1 molar ratio (citric acid : nitrates). The mixture was homogenized by stirring at 400 rpm for 30 min and dried at 60 °C for 12 h, yielding a transparent gel. This gel was ignited in a quartz beaker within a furnace preheated to 800 °C, a temperature critical for phase purity and particle size control.[24] The gel rapidly expanded ~10-fold into a voluminous, black, fluffy mass, releasing CO_2 and H_2O vapors. Within 15–30 min, combustion produced a white YSZO:Eu^{3+} nanopowder with a yield ~95%, consistent with a scalable sol–gel combustion route. The friable product was ground into a fine powder for characterization. The above synthesis process and images of the final product under ambient and UV illumination are displayed in Fig. S1. This rapid, efficient synthesis delivers uniform, Eu^{3+}-activated nanopowders with exceptional optical properties, poised for advanced nanotechnology applications.

2.2. Materials characterization

The phase purity and crystallographic structure of the YSZO:Eu^{3+} nanopowders were elucidated using powder X-ray diffraction (PXRD, X'Pert, Cu Kα radiation, λ = 1.5406 Å), with data refined *via* the WIN INDEX software.[25] Morphological features and elemental composition were probed using a field-emission scanning electron microscope (FESEM, Nova NanoSEM 450), coupled with energy-dispersive X-ray spectroscopy (EDS), revealing nanoscale uniformity and dopant distribution.[26] Atomic-level lattice configuration and internal structure were investigated through high-resolution transmission electron microscopy (HRTEM, TECNAI-12, 120 kV), unveiling intricate nanoscale details that are critical to performance. Photoluminescent properties were characterized using a fluorescence spectrophotometer (Hitachi F-4700) equipped with a xenon arc lamp, capturing excitation and emission spectra to assess the nanopowders' triple-excitable luminescence and optical excellence. The esterification product was characterized using Fourier transform infrared spectroscopy (FTIR, Bruker, alpha II) to identify its functional groups. These advanced techniques collectively affirm the structural integrity, morphological precision, and luminescent prowess of the YSZO:Eu^{3+} nanomaterials, underpinning their nanotechnology-driven applications.

2.3. Preparation of luminescent inks

Luminescent security inks were engineered by integrating YSZO:0.2Eu^{3+} nanopowders into a transparent polymer matrix. Polyvinyl alcohol (PVA, Sigma-Aldrich, ≥99%) was dissolved in deionized water (18.2 MΩ cm) under vigorous stirring (500 rpm) at 80 °C for 1 h, yielding a homogeneous PVA solution.[27] Oleic acid (1, 3, or 5 parts per hundred, pph) was then incorporated as a surfactant, followed by *p*-toluenesulfonic acid (*p*-TSA, ≥98%) as a catalyst, with the mixture stirred at 100 °C for 30 min to ensure uniformity. After cooling to ambient temperature, YSZO:0.2Eu^{3+} nanopowders were dispersed into this matrix with (1 : 5 wt%) *via* high-speed stirring (1000 rpm) for 15 min, producing a stable, fluorescent nano-ink with exceptional optical clarity.[28] The details of the preparation of the luminescent ink and the probable reaction of PVA and oleic acid are shown in Fig. S1 and S2. The resulting ink was applied to diverse substrates, including paper, plastic, and glass, using dip-pen writing, brushing, and screen-printing techniques to encode covert patterns. These encrypted features, invisible

under ambient light, were vividly revealed under a UV lamp (254 nm), showcasing the ink's nanoscale luminescent prowess for advanced security applications.[29,30]

3. Results and discussion

3.1. Structural analysis

The powder X-ray diffraction (PXRD) pattern of bulk and nanopowders of YSZO:(0-0.3Eu^{3+}), depicted in Fig. 1(a), reveals no significant structural perturbation upon Eu^{3+} doping.[25,31,32] To confirm and identify the phase and crystallinity, bulk YSZO:(0-0.2)Eu^{3+} was synthesized using a solid-state method because the material of interest, YSZO, is a new lattice, and no JCPDS/ICDD data were available. Given the comparable ionic radii of Eu^{3+} (0.106 nm) and Y^{3+} (0.101 nm), Eu^{3+} ions seamlessly occupy Y^{3+} sites within the YSZO lattice, with a percentage difference in ionic radii (Δr) of ~5%, well below the 15% threshold for effective substitution.[33,34] This can be written as follows:

$$\Delta r = \frac{R_h(\mathrm{CN}) - R_d(\mathrm{CN})}{R_h(\mathrm{CN})} \times 100 \quad (1)$$

where, R_h and R_d are the ionic radii of the dopant ions and the host cation, respectively, and CN is the coordination number. The Δr value was found to be around 4.95% less than 15%. This confirms successful Eu^{3+} incorporation into the host matrix. As YSZO represents a novel nanoscale lattice absent from JCPDS records, a bulk YSZO reference was synthesized *via* solid-state reaction to validate phase purity and crystallinity. Structural analysis using WIN-INDEX (v3.08) software elucidated (*hkl*) planes, affirming an orthorhombic Pbnm space group with unit cell parameters: a = 0.753 nm, b = 1.264 nm, c = 0.531 nm, and volume = 50.54 nm^3. Crystallite size, derived from the Scherrer equation, averaged 22 nm for the sol–gel combustion-synthesized nanopowders, underscoring their nanoscale uniformity. Fig. S3 displays the predicted crystal structure of YSZO NPs in a ball-stick model.

Eqn (2) represents Scherrer's formula, which was used to yield the material's crystallite size.[35]

$$D = \frac{0.9\lambda}{\beta \cos\theta} \quad (2)$$

where, λ is the X-ray wavelength, β is the FWHM, θ is the Bragg angle, D is the average crystallite size, and K is the dimensionless form factor (0.9). This highlights the structural integrity and substitution efficacy of YSZO:Eu^{3+}, positioning it as a robust platform for nanotechnology-driven applications.

3.2. Morphological studies

Surface morphology critically governs the functionality of nanomaterials, particularly for anticounterfeiting applications. Field-emission scanning electron microscopy (FESEM) images of YSZO:0.2Eu^{3+} nanopowders, presented in Fig. 1(b), reveal a uniform ensemble of agglomerated spherical and oval nanoparticles, averaging 200 nm in size.[36] This nanoscale uniformity enhances their suitability for security ink formulations. Energy-dispersive X-ray spectroscopy (EDS) and elemental mapping, shown in Fig. 1(c), confirm the presence of all expected elements with proportional distribution and no detectable impurities, underscoring the compositional purity. High-resolution transmission electron microscopy (HRTEM), depicted in Fig. 1(e), unveils an interplanar spacing (d) of ~0.36 nm and a slightly larger average particle size of 250 nm, reflecting synthesis-dependent variability. The polycrystalline nature of the nanopowders is evidenced by the selected area electron diffraction (SAED) patterns shown in Fig. 1(d). Morphology and

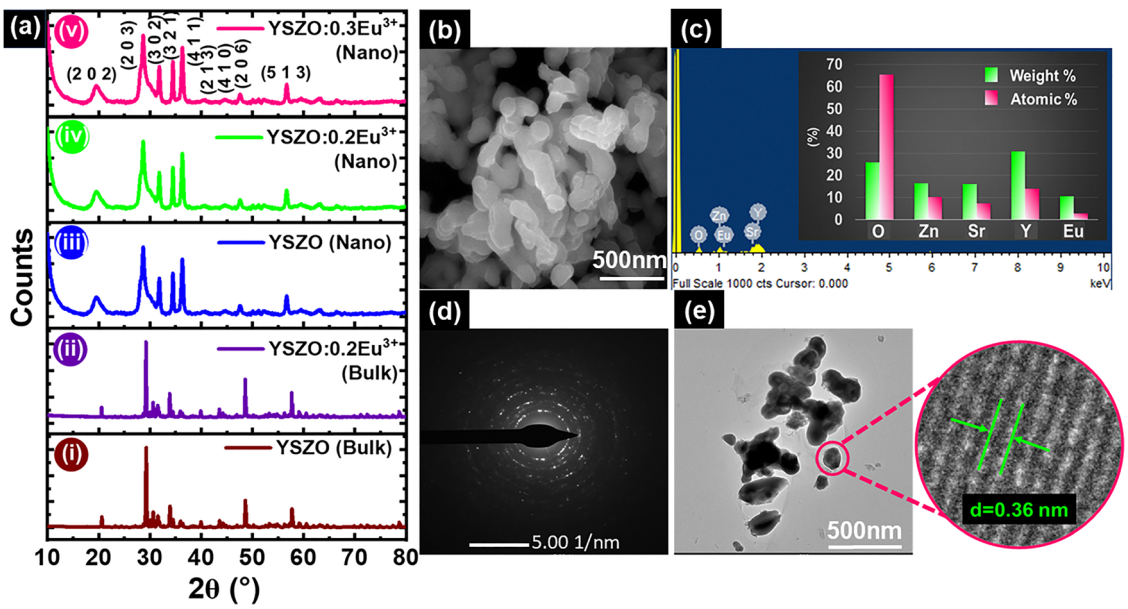

Fig. 1 (a) Powder XRD patterns of (i) bulk undoped (YSZO), (ii) bulk doped (YSZO:Eu^{3+}), and (iii)–(v) undoped and doped nanopowders. (b) Scanning electron micrograph, (c) EDAX spectra, (d) SAED pattern, and (e) HRTEM image of YSZO:0.2Eu^{3+} NPs.

particle size are influenced by precursor states, reaction temperature, and the sol–gel combustion process, affirming synthetic control over nanoscale features. This validates the successful fabrication of YSZO:0.2Eu^{3+} nanopowders, positioning them as a robust platform for advanced security applications.

3.3. Photoluminescence studies

The photoluminescence (PL) properties of YSZO:Eu^{3+} nanopowders, pivotal to their anticounterfeiting potential, are comprehensively elucidated in Fig. 2. Fig. 2(a) depicts the excitation spectra, spanning 220–500 nm, which reveal a broad ultraviolet band (220–280 nm) attributed to charge transfer (CT) between Eu^{3+} and O^{2-}, underscoring efficient energy absorption at the nanoscale.[37] Sharp intra-4f transitions at 393 nm ($^7F_0 \rightarrow {}^5L_6$), 415 nm ($^7F_0 \rightarrow {}^5D_3$), and 465 nm ($^7F_0 \rightarrow {}^5D_2$) confirming Eu^{3+} incorporation. This triple-excitable nature, spanning UV, near-UV, and blue regions, renders these nanopowders exceptionally versatile for security ink applications, enabling activation across multiple wavelengths. As shown in Fig. 2(b), the emission spectra recorded in the 550–750 nm range exhibit strong peaks at 595 nm ($^5D_0 \rightarrow {}^7F_1$) and 612 nm ($^5D_0 \rightarrow {}^7F_2$), corresponding to the characteristic red emission of Eu^{3+} ions.

According to the selection criteria, magnetic dipole (MD) transition is typically permitted while electric dipole (ED) transition is prohibited. The crystal field's odd parity constituent in YSZO:Eu^{3+}, however, partially facilitated the forbidden ED transition ($^5D_0 \rightarrow {}^7F_2$). At 654 and 710 nm, two weak emission bands were identified as $^5D_0 \rightarrow {}^7F_3$ and $^7F_4$, respectively. The intensity distribution of transitions from $^5D_0$ to ^7F_J (where J = 0, 1, 2, and 3) is solely dependent on the Eu^{3+} ion's local surrounding symmetry.[38] A few transitions have this characteristic, making them hypersensitive to the crystal environment. These transitions are considered to be hypersensitive because the ligand ions in the host have a significant influence on their intensity.[39] In this case, there is less MD transition between $^5D_0$ and $^7F_1$, while there is a hypersensitive ED transition between $^5D_0$ and $^7F_2$. While the shape of the emission band remains constant, the emission intensities of the observed bands vary in response to changes in Eu^{3+} ion concentrations. Since the 4f electrons are protected by the external electric fields of the outer electrons, it is widely known that ligand ions in crystals have a negligible effect on the energy levels of the trivalent lanthanides.[40] Under 254 nm excitation, the shift of emission intensity with dopant concentration in the range of 0–0.3 mol is depicted in Fig. 2(b). All of the detected emission bands show an increase in intensity as the concentration of Eu^{3+} rises.

This is attributed to energy migration between activators up to a 0.2 mol threshold, after which the killer site is ultimately reached by a quenching mechanism linked to exchange contact. The distance between the activator ions decreases as the concentration of activator ions increases, indicating an energy exchange between them. The $^5D_0 \rightarrow {}^7F_2$ (ED) transition at

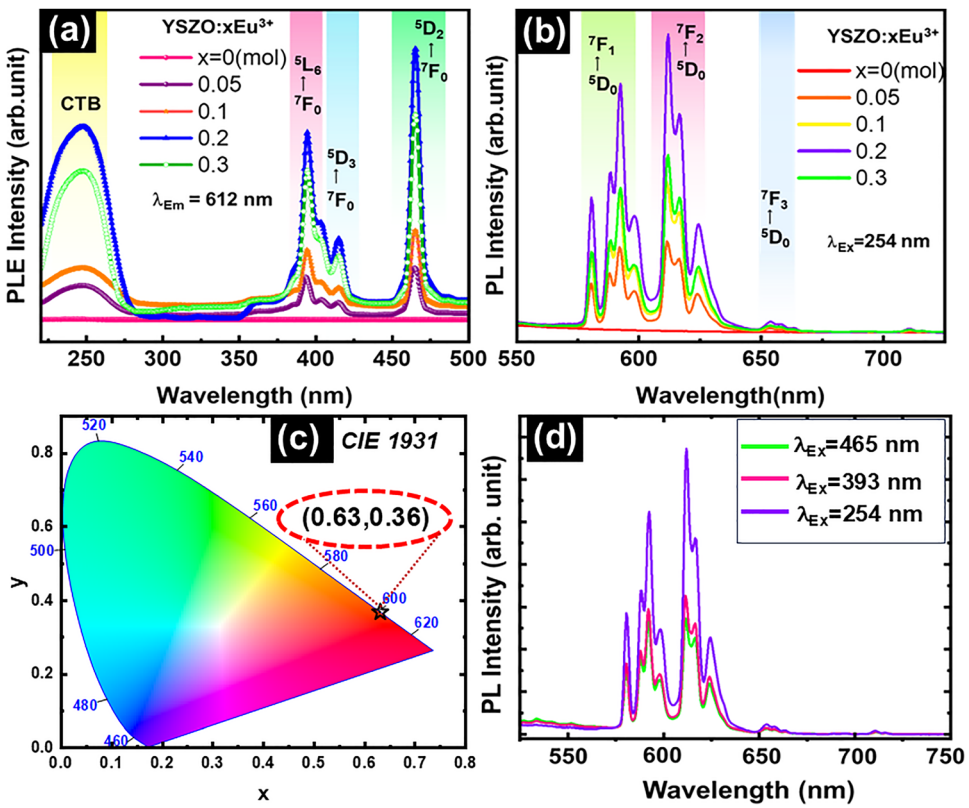

Fig. 2 (a) PL excitation and (b) PL emission spectra of YSZO:x(0-0.3) Eu^{3+} NPs. (c) CIE chromaticity diagram. (d) PL emission spectra recorded at 254, 393, and 465 nm.

Table 1 Asymmetric ratio of YSZO:xEu^{3+} (x = 0.05–0.2 mol) NPs

S. no.	Conc. of Eu^{3+} doped in the YSZO lattice (mol)	Asymmetric ratio
1	0.05	1.06
2	0.1	1.23
3	0.2	1.32
4	0.3	1.2

612 nm in the current work has a higher emission intensity than the $^5D_0 \rightarrow {}^7F_1$ (MD) transition at 595 nm.

Table 1 presents the asymmetry ratio (ED/MD integrated intensity) of YSZO : xEu^{3+} nanoparticles (x = 0.05–0.2 mol). The asymmetry ratio increases with Eu^{3+} doping concentration, reaching an optimum at 0.2 mol Eu^{3+}. This trend indicates maximum site asymmetry and enhanced luminescent efficiency at the highest doping level.[41,42] Fig. 2(c) depicts the CIE chromaticity coordinates (x = 0.63, y = 0.36), which place the emission in the pure-red region, with a remarkable color purity of 99.82%, affirming the nanopowders' optical excellence for nanoscale security features.[43] These findings highlight YSZO:Eu^{3+} as a photoluminescent powerhouse, merging triple excitability, high purity, and concentration-tuned intensity for cutting-edge applications. Fig. 2(d) shows the PL spectra of YSZO:0.2Eu^{3+} under 254 nm, 393 nm, and 465 nm, revealing that the intensity under 254 nm is brighter than at the other two excitation wavelengths. So, we have used the 254 nm UV lamp for the application. Table 2 depicts the relative quantum efficiency of YSZO:0.2Eu^{3+} NPs and compares them with those of commercial red phosphors.

Fluorescent decay measurements unveiled the fluorescence lifetime dynamics of YSZO:Eu^{3+} nanopowders, a critical metric for their anticounterfeiting efficacy.[44] The decay profile of the $^5D_0$ level of Eu^{3+}, corresponding to the dominant $^5D_0 \rightarrow {}^7F_2$ transition at 612 nm, is showcased in Fig. 3 for YSZO:0.2Eu^{3+}. Measured with an excitation wavelength of 254 nm and emission fixed at 612 nm, the lifetime reflects the temporal behavior of radiative recombination in this nanoscale system. The measured decay curve follows the mathematical expression below.

$$I = I_0 \exp\left(-\frac{t}{\tau}\right) \quad (3)$$

where I_0 is the initial intensity, *i.e.*, at t = 0, I is the intensity at any time t, and τ is the fluorescence lifetime of the Eu^{3+}-doped YSZO powder.

The decay curve exhibits a single-exponential fit, indicative of uniform radiative relaxation between Eu^{3+} electrons and holes, devoid of non-radiative pathways that plague less stable nanomaterials. The fitted lifetime of 0.72 ms surpasses those of typical fluorescent materials (~10 ns), highlighting an exceptionally prolonged excited-state persistence, attributable to the robust YSZO lattice and Eu^{3+} coordination environment.[45,46]

Table 2 Relative quantum efficiency (QE) of the synthesized YSZO:Eu^{3+} NPs and commercial phosphors

Phosphor name	λ_{Ex} (nm)	λ_{Em} (nm)	QE (%)
Commercial CREE (Y_2O_3:Eu^{3+})	254	612	78
	393	612	<1
	465	612	<1
Current work (Y_2SrZnO_5:Eu^{3+})	254	612	87.3
	393	612	41
	465	612	56

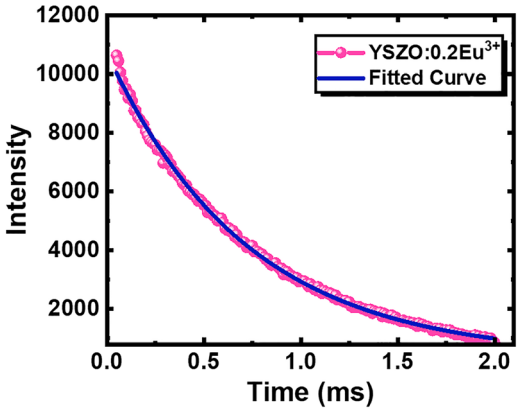

Fig. 3 Fluorescent decay curve of YSZO:0.2Eu^{3+} NPs.

Temperature-dependent photoluminescence (TDPL) studies, depicted in Fig. 4(a) and (b), unravel the thermal resilience and emission sensitivity of YSZO:Eu^{3+} nanopowders and their security ink derivatives across a 40–160 °C range, a critical parameter for nanoscale anticounterfeiting applications. The emission peak at 612 nm ($^5D_0 \rightarrow {}^7F_2$) remains steadfast in position, yet its intensity progressively diminishes with rising temperature, reflecting a controlled transition from radiative to nonradiative pathways.[47] The YSZO:Eu^{3+} nanopowders exhibit remarkable luminous thermal stability, retaining 80.5% of their room-temperature photoluminescence (PL) intensity at 160 °C, as evidenced in the inset of Fig. 4(a) and (b).[48] This minor attenuation results from the diversion of excitation energy from the luminescent Eu^{3+} core to nonradiative thermal emission through lattice relaxation, with phonon-assisted processes increasingly prevalent at elevated temperatures, thereby reducing PL efficiency.[49] Additionally, the spectroscopic behavior of YSZO:Eu^{3+} integrated with non-aqueous polymers (polycarbonate, polystyrene, and polymethyl methacrylate) is comprehensively detailed in the supplementary data (S4), underscoring their potential for advanced anticounterfeiting applications.

Fourier-transform infrared (FTIR) spectroscopy reveals distinct differences between pure polyvinyl alcohol (PVA) and its oleic acid (OA) ester, unequivocally confirming successful modification. In Fig. 5(a), the FTIR spectrum of pure PVA displays a broad absorption band at 3457 cm^{-1}, attributed to –OH stretching, indicative of abundant hydroxyl groups. Peaks at 2935 cm^{-1} correspond to aliphatic C–H stretching, while absorptions at 1380, 1239, and 1093 cm^{-1} signify C–H bending and C–O stretching within the polymer backbone. The absence of absorption in the 1700–1750 cm^{-1} region verifies the complete hydrolysis of PVA, ruling out ester functionalities. In contrast, Fig. 5(b) reveals a prominent peak at 1711 cm^{-1}, characteristic of a carbonyl group. Following esterification with oleic acid, as shown in Fig. 5(c), the –OH band shifts to

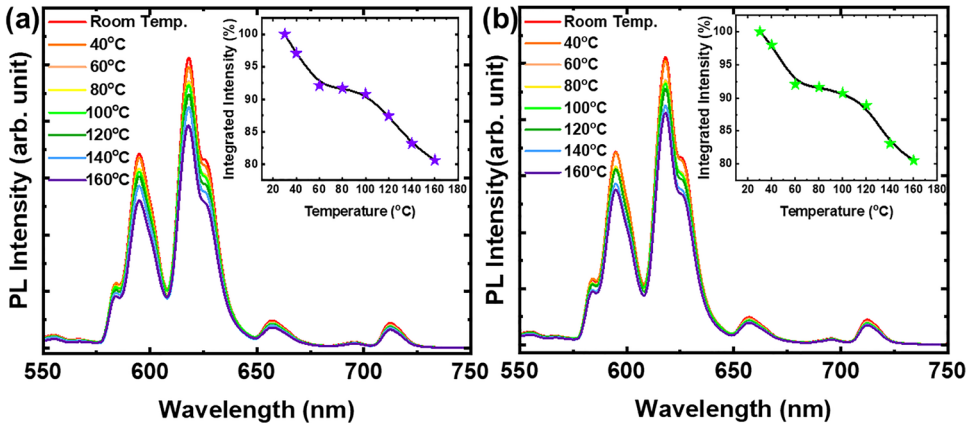

Fig. 4 (a) TDPL emission spectra of YSZO NPs; inset: integrated intensities as a function of temperature for a heating cycle. (b) TDPL emission spectra of YSZO security ink; inset: integrated intensities as a function of temperature for a heating cycle.

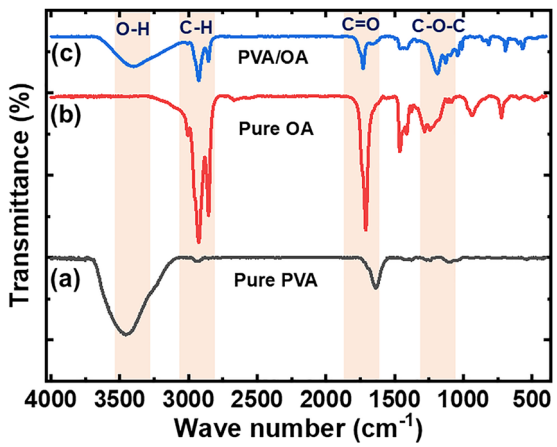

Fig. 5 FTIR spectra of (a) pure PVA, (b) pure OA, and (c) modified PVA/OA.

3399 cm^{-1} with reduced intensity, indicating partial hydroxyl consumption. New, robust peaks at 3000, 2925, and 2855 cm^{-1} correspond to the hydrocarbon chain of oleic acid, while a distinct band at 1730 cm^{-1} confirms ester carbonyl formation. Additional peaks at 1600, 1459, and 1187–1012 cm^{-1} further substantiate the successful incorporation of oleic acid, underscoring the modified material's suitability for advanced nanoink matrices.[50,51]

3.4. Security ink applications

The escalating prevalence of counterfeiting, spanning certificates, currency, tickets, checks, and trademarks, has propelled anticounterfeiting technologies to the forefront of global security efforts. Among these, fluorescent nanopowder-based systems, exemplified by YSZO:Eu^{3+}, have emerged as luminaries due to their unparalleled concealment and vivid emission properties, outshining conventional methods. In an era of advancing threats, ink stability emerges as a linchpin, fortifying resilience against sophisticated forgery while preserving authenticity across diverse conditions.[52] To this end,

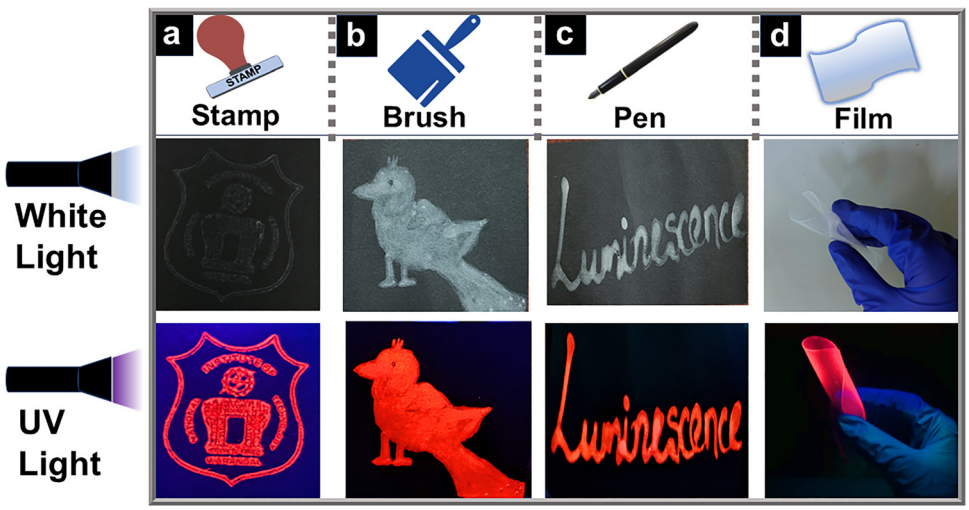

Fig. 6 (a)–(c) Anti-counterfeiting labels painted with YSZO:0.2Eu^{3+} fluorescent ink in 3 different ways. (d) Transparent film with excellent flexibility and foldability under white light and UV (254 nm) light.

YSZO:0.2Eu^{3+} nanopowders were seamlessly integrated into a polyvinyl alcohol–oleic acid (PVA–OA) matrix, yielding a highly translucent, viscous nanoink. This versatile nanoink adapts effortlessly to multiple printing modalities such as gravure, letterpress, dip-pen writing, and screen printing demonstrating exceptional applicability. In Fig. 6(a)–(c), digital images under ambient and 254 nm UV light reveal striking contrasts: brush and dip-pen patterns, rich in YSZO:0.2Eu^{3+} content, exhibit intense red emission that is sharp and discernible, while stamp-mode patterns remain concealed under white light and unveil their brilliance only under UV stimulation.[53] This selective visibility underscores the ink's efficacy as a covert anticounterfeiting tool. A schematic in Fig. 6(d) further illustrates a facile UV-stimulated patterning method, casting the ink into a transparent, flexible film. Under 254 nm UV light, this film showcases vivid red luminescence, exceptional foldability, and durability, hallmarks of a nanotechnology-driven security solution.[54] These attributes of stability, adaptability, and concealable luminescence position YSZO:Eu^{3+} nanoinks as a transformative platform, redefining anticounterfeiting in an age of relentless innovation and forgery. In stamp mode, the ink is not visible properly (transparent pattern) under white light, but when brushing and writing, patterns are visible since the content of YSZO:0.2Eu^{3+} NPs is increased.

The escalating prevalence of forgeries, encompassing documents such as certificates, currency, and trademarks, has intensified the demand for robust anti-counterfeiting measures in recent years.[55,56] Within this evolving landscape of security challenges, the stability of security inks stands as a pivotal factor, underpinning their efficacy in preventing counterfeiting and ensuring authenticity.[57] The incorporation of innovative additives and advanced encapsulation technologies markedly enhances ink stability, prolonging durability and bolstering resilience against a wide array of threats.

3.4.1 QR and bar code detection. The unprecedented YSZO:Eu^{3+} nanopowders unlock transformative anticounterfeiting applications, and their luminescent prowess can be extended to barcodes, quick response (QR) codes, and banknotes. To ensure a stable colloidal suspension, YSZO:Eu^{3+} was meticulously blended with a PVA–OA matrix in a dry, dust-free environment, optimizing nanoscale dispersion for security encoding. Fig. 7 showcases a sample QR code, its iconic black-and-white grid concealing encrypted data such as website URLs and error correction levels beneath a sophisticated masking pattern.[58] Every code contains some secret data about a particular website and the error repair level status. The QR code's use of an encrypting disguise over its information is another unique characteristic. The type of mask employed and the data to be saved determine each QR code's active region. The assurance of text readability is provided by the removal of large sections of darkened or repetitive white modules. Three square boxes that act as anchors and provide a safe layout for

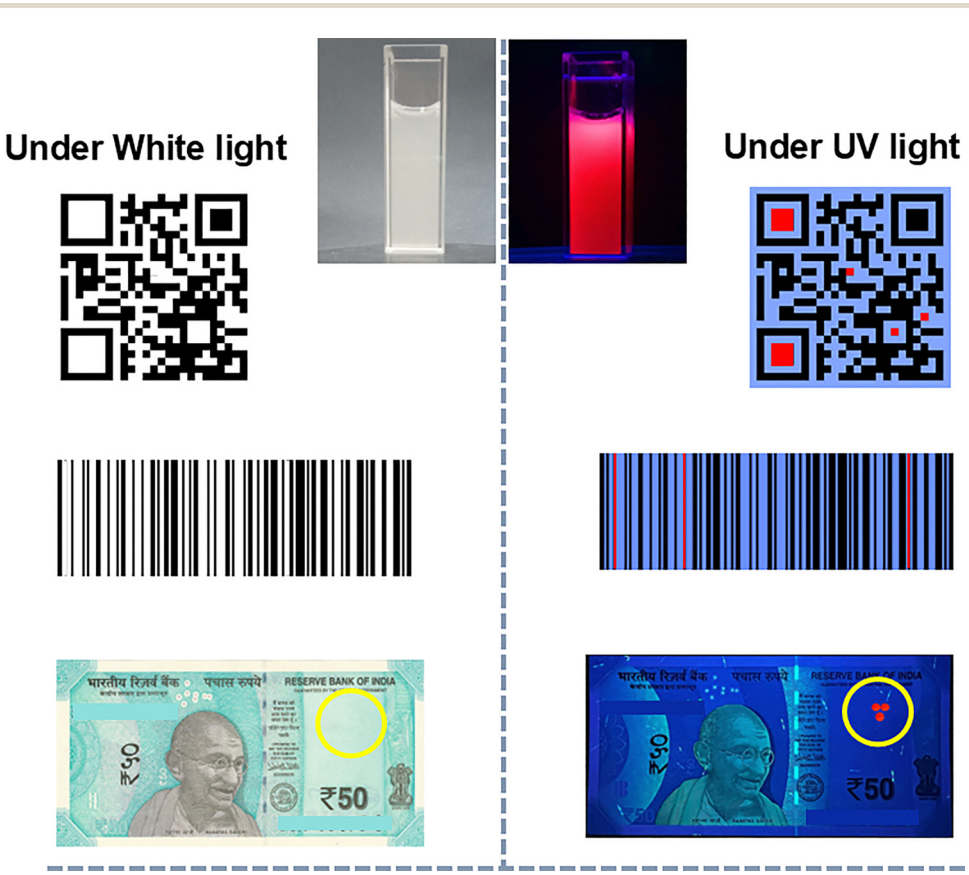

Fig. 7 Optical images of a QR code, bar code, and Indian currency protected by YSZO NPs security ink under the exposure of UV light of ~254 nm.

quick reading are positioned in the bottom, upper left, and upper right corners. The smaller black blocks are scattered across the code, starting in the lower right corner, depending on the version used to create the QR code. It is interesting to note that the timing pattern, which is indicated by the top left anchors, is separated by a column of modules that alternate between black and white as well as a row of dark segments between the top right and top left anchors. To the left of the top right anchor and above the bottom left anchor is information regarding the version that was utilised. Formatting informations such as error correction level and the mask pattern, are positioned near the top-left and top-right anchors and adjacent to the right side of the bottom-left anchor. These are the fundamental characteristics that help us recognise, categorise, and standardise QR codes. Unlike traditional QR codes, which are limited to a few thousand alphanumeric characters, YSZO:Eu^{3+}-enhanced variants transcend these constraints, merging high-capacity storage with covert luminescent security.[59,60]

Under ambient light, these nanoink-printed QR codes, barcodes, and currency remain invisible, their blocks, lines, and dots, respectively, cloaked from the naked eye. However, illumination at 254 nm UV unveils a vivid red emission (~612 nm) from the YSZO:Eu^{3+} coding channels, as captured in the optical images shown in Fig. 7, rendering hidden patterns detectable only with specialized equipment. This fluorescence fortifies data integrity, safeguarding information against forgery. For barcodes, YSZO:Eu^{3+} elevates both one-dimensional (1-D) and two-dimensional (2-D) systems. The 1-D system relies on line-width variations for product identification, and the 2-D system embeds richer descriptions *via* symbols. The UV-stimulated luminescence of the nanopowders adds a robust security layer to 2-D barcodes, enhancing storage, readability, and authenticity over conventional designs.[58] By integrating nanoscale photoluminescence with multi-layered encoding, YSZO:Eu^{3+} redefines QR and barcode detection, offering a cutting-edge, nanotechnology-driven shield against counterfeiting in an increasingly digital landscape.

3.4.2 Humidity stability of luminescent ink. The humidity stability of luminescent security inks is paramount to their efficacy, particularly for preserving nanoscale anticounterfeiting features embedded in documents and high-value items exposed to diverse environmental challenges.[61] Unlike conventional inks, which are susceptible to moisture-induced degradation or reactivity, YSZO:Eu^{3+} nanoinks must deliver unwavering performance to prevent false positives or negatives, thereby ensuring the authenticity and integrity of encoded patterns throughout their lifecycle. Humidity presents a significant challenge, potentially causing color bleaching, color shifts, or luminescence quenching, which could undermine the reliability of security features in real-world applications.[62]

To evaluate this resilience, YSZO:Eu^{3+}-infused polyvinyl alcohol–oleic acid (PVA–OA) films, formulated with varying oleic acid concentrations (1, 3, and 5 parts per hundred, pph), were subjected to a rigorous 24-hour test in a humidity-regulated chamber at 100% relative humidity (RH). The moisture content and PL intensity were meticulously monitored at intervals, as illustrated in Fig. 8(a). The 5 pph OA variant demonstrated exceptional water resistance, exhibiting no detectable alteration in PL intensity over time. This outstanding stability is attributed to the hydrophobic long-chain structure of oleic acid, which reinforces the PVA matrix against moisture ingress, thereby safeguarding the nanoscale luminescent core

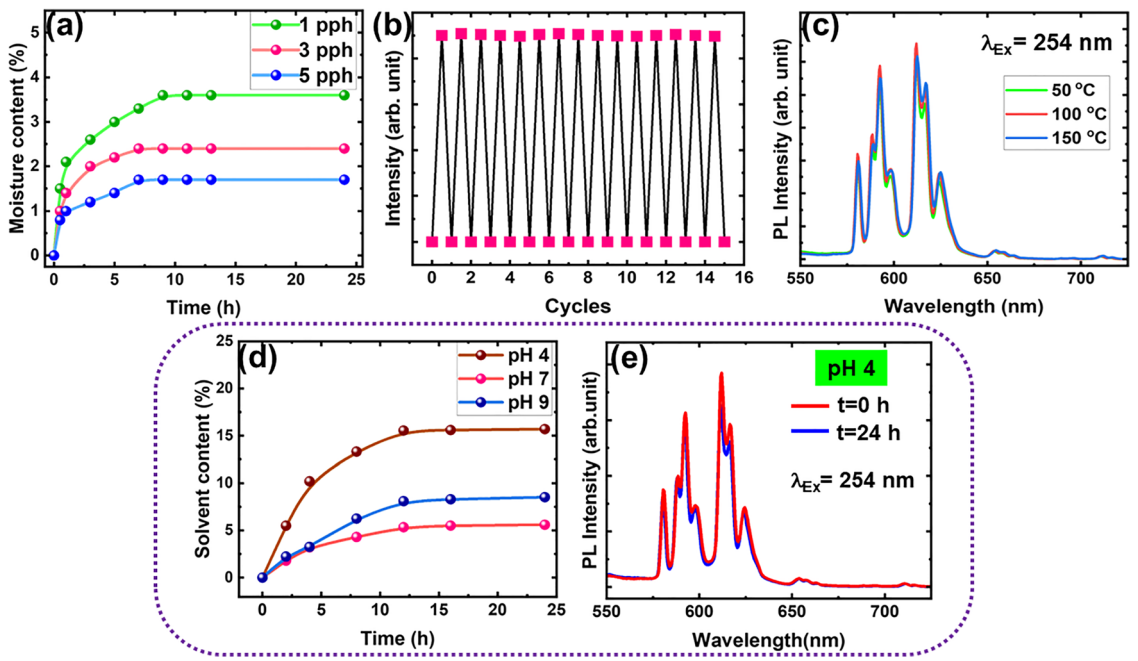

Fig. 8 (a) Moisture content in the film w.r.t time, (b) reversibility at 612 nm after each UV excitation cycle, (c) PL spectra of the films thermally cured for 24 hours at different temperatures, (d) solvent content in the film w.r.t time, and (e) PL spectra of the film dipped into a buffer solution of pH 4.

of YSZO:Eu^{3+}. The consistent red emission at 612 nm under 254 nm UV excitation, which was unaffected by prolonged humidity exposure, underscores the ink's robustness, distinguishing it from less resilient systems.[63] This introduces YSZO:Eu^{3+} nanoink as a paradigm of environmental endurance, delivering uncompromising luminescent fidelity for cutting-edge security applications under the most demanding conditions.

3.4.3 Photostability of luminescent ink. Photostability is a cornerstone of YSZO:Eu^{3+}-based nanoinks, ensuring that security markings and nanoscale features withstand prolonged light exposure, particularly UV irradiation, without fading or degradation.[64] This resilience is critical for maintaining the longevity and legibility of encoded elements such as holograms, watermarks, and luminescent patterns that underpin the authenticity of secure documents. Unmitigated photodegradation could compromise these features, eroding the reliability of anti-counterfeiting systems over time. By prioritizing photostability in the design and validation of YSZO:Eu^{3+} nanoinks, these materials emerge as a robust defense against environmental stressors, thwarting forgery attempts and ensuring the integrity of high-stakes applications.

To evaluate this durability, YSZO:Eu^{3+}-infused PVA–OA films were subjected to a rigorous cyclic UV exposure regimen. The films were irradiated with 254 nm UV light (8 W) at ambient temperature for 5-hour cycles, followed by periods of darkness to revert to their white state, over 15 consecutive cycles. Post-irradiation, the films exhibited vibrant red emission at ~612 nm, seamlessly returning to their ambient white appearance in darkness, demonstrating a dynamic photoresponse. In Fig. 8(b), PL intensity, monitored after each cycle, showed exceptional consistency with no detectable decline across all cycles. Furthermore, the CIE chromaticity coordinates ($x = 0.63$, $y = 0.36$) and the color purity of 99.82% remained unwavering, underscoring the nanoinks' superior photostability. This robust performance is attributed to the resilient lattice of YSZO:Eu^{3+} nanopowders, which effectively shields the luminescent core from UV-induced degradation, setting these nanoinks apart from their less stable counterparts. This establishes YSZO:Eu^{3+} nanoink as a photostable powerhouse, delivering enduring luminescence and reliability for advanced nanoscale security applications.[65]

3.4.4 Thermal stability of luminescent ink. Luminescent thermal stability is a pivotal attribute of YSZO:Eu^{3+} nanoinks, ensuring their ability to withstand elevated temperatures while preserving the integrity of luminescent security features. Such resilience is critical, as thermal instability could lead to melting, discoloration, or degradation of nanoscale-encoded patterns, compromising document authenticity and enabling heat-based tampering.[66] In advanced security printing, where inks incorporate specialized pigments or dyes to reveal covert features or indicate interference under thermal stress, robust stability guarantees reliability across manufacturing processes and real-world conditions. Rigorous luminescent thermal stability testing is thus essential in nanoink development, reinforcing these systems against counterfeiting strategies that exploit thermal vulnerabilities.

To assess this durability, YSZO:Eu^{3+}-infused PVA–OA films were subjected to thermal curing at 50, 100, and 150 °C for 24 hours, with the PL intensities meticulously recorded post-exposure, as shown in Fig. 8(c). The films demonstrated remarkable consistency, maintaining vibrant red emission at 612 nm with negligible deviation up to 100 °C, reflecting the robust lattice stability of the nanopowders.[67] At 150 °C, a subtle change was observed: while PL intensity remained largely preserved, the film exhibited a slight yellowish-brown discoloration, likely due to minor oxidation of the polymer matrix rather than degradation of the YSZO:Eu^{3+} luminescent core. This exceptional thermal resilience, preserving optical fidelity under significant heat stress, distinguishes YSZO:Eu^{3+} nanoinks from less stable alternatives, confirming their suitability for security applications where durability is paramount.[68] This underscores a nanotechnology-driven breakthrough, combining thermal fortitude with luminescent precision to strengthen anti-counterfeiting measures.

3.4.5 Solvent stability of luminescent ink. Solvent stability is a critical attribute of YSZO:Eu^{3+} nanoinks, underpinning their resilience against diverse solvent exposures encountered in security printing and real-world applications. These inks face constant challenges from cleaning agents, environmental contaminants, and incidental substances, necessitating robust stability to prevent detrimental effects such as fading, color shifts, or luminescence quenching.[69] This durability ensures that nanoscale security features, such as encoded patterns, QR codes, and luminescent markers, maintain optical fidelity and functional integrity over time, meeting the stringent requirements of precision-driven industries, such as anti-counterfeiting and packaging. Consequently, solvent stability testing is a cornerstone of quality control, revealing formulation vulnerabilities and guiding enhancements to improve durability and align with the rigorous demands of advanced printing technologies.

To evaluate this robustness, YSZO:Eu^{3+}-infused PVA–OA films were subjected to immersion in buffer solutions across a pH range (4, 7, and 9) for 24 hours, with PL intensities and solvent uptake meticulously monitored at regular intervals, as shown in Fig. 8(d) and (e). The films demonstrated exceptional stability, retaining their intense red emission at 612 nm without detectable attenuation, even after extended exposure.[70] Solvent uptake analysis revealed minimal penetration, attributed to the hydrophobic reinforcement provided by oleic acid within the PVA matrix, which effectively shields the YSZO:Eu^{3+} luminescent core from chemical degradation. This remarkable stability sets YSZO:Eu^{3+} nanoinks apart from less resilient formulations, confirming their ability to preserve nanoscale-encoded authenticity under solvent stress. This highlights a significant advancement in nanotechnology, delivering a solvent-stable luminescent platform that strengthens anti-counterfeiting measures with unmatched reliability and longevity.

4. Conclusions

In summary, this study unveils a groundbreaking Eu^{3+}-activated Y_2SrZnO_5 (YSZO) nanoink, synthesized *via* an

optimized sol–gel combustion technique, that outshines conventional luminescent security inks for currency and classified documents. The resulting nanopowders exhibit an orthorhombic Pbnm structure, adorned with uniform spherical and oval morphologies, and deliver a dominant red emission at 612 nm, as revealed by PL spectra. Demonstrating triple excitability at 254 (UV), 393 (near-UV), and 465 nm (blue), these nanopowders emit a vivid red glow with an exceptional color purity of 99.8%, underpinned by Eu^{3+} ions occupying low-symmetry sites within the YSZO lattice. Concentration quenching, mediated by exchange interactions, peaks at an optimal Eu^{3+} doping of 0.2 mol, maximizing luminescent efficiency. A robust security ink was engineered by integrating YSZO:Eu^{3+} with a modified PVA–oleic acid (PVA–OA) matrix, catalyzed by *p*-TSA, yielding a formulation that excels in stability. This nanoink withstands a gauntlet of environmental challenges, including aging, humidity, UV irradiation, thermal stress, and solvent exposure, preserving its luminescent fidelity and structural integrity over extended periods. Transparent under ambient light yet brilliantly responsive under UV, the ink's resilience ensures the reliability and authenticity of printed security features amidst evolving threats. By addressing formulation complexities and stability hurdles, this work underscores the transformative potential of YSZO:Eu^{3+} nanoinks, heralding a new era of nanotechnology-driven anticounterfeiting solutions with unparalleled precision and durability.

Author contributions

Payal P. Pradhan: data curing, methodology, writing – original draft. Tejaswi Jella: data curation, formal analysis. M. Rakshita: data curation, formal analysis. Aachal A. Sharma: data curation, investigation. K. A. K. Durga Prasad: data curation, investigation. D. Haranath: conceptualization, funding acquisition, methodology, supervision, writing – review and editing.

Conflicts of interest

There are no conflicts of interest to declare.

Data availability

The data supporting the findings of this study are available from the corresponding author upon reasonable request. Any requests for data should specify the purpose and scope of the inquiry to facilitate review and approval.

Supplementary information is available. See DOI: **https://doi.org/10.1039/d5tc02801a**.

Acknowledgements

The authors AAS, MR and TJ thank the Department of Science and Technology (DST), the Government of India's Council of Scientific & Industrial Research (CSIR) and Institute Post-Doctoral Fellowship, National Institute of Technology Warangal, India for financial support through various projects *viz.* INSPIRE scheme #IF200233, CSIR-JRF #09/0922(11518)/2021-EMR-I, and NITW/AD-3/PDF/2022/1209 respectively.

References

1 OECD Economic Outlook, 2023.
2 P. Kumar, D. Singh and I. Gupta, *J. Alloys Compd.*, 2023, **966**, 171410.
3 D. Xu, D. Haranath, H. He, S. Mishra, I. Bharti, D. Yadav, B. Sivaiah, B. Gahtori, N. Vijayan, A. Dhar, J. Zhu, V. Shanker and R. Pandey, *CrystEngComm*, 2014, **16**, 1652–1658.
4 A. A. Elrowayati, M. A. Alrshah, M. F. L. Abdullah and R. Latip, *IEEE Access*, 2020, **8**, 114172.
5 R. Arppe and T. J. Sørensen, *Nat. Rev. Chem.*, 2017, **1**, 31.
6 H. Chen, H. Hu, B. Sun, H. Zhao, Y. Qie, Z. Luo, Y. Pan, W. Chen, L. Lin, K. Yang, T. Guo and F. Li, *ACS Appl. Mater. Interfaces*, 2023, **15**, 2104–2111.
7 S. A. Ahson and M. Ilyas, *RFID handbook: applications, technology, security, and privacy*, CRC press, 2017.
8 L. O'Gorman and I. Rabinovich, *IEEE Trans. Pattern Anal. Mach. Intell.*, 1998, **20**, 1097–1102.
9 K. Muthamma, B. E. Pallavi, D. Sunil, S. D. Kulkarni, S. Wagle and D. Kekuda, *Colloids Surf., A*, 2022, **653**, 129910.
10 Y. Sun, X. Le, S. Zhou and T. Chen, *Adv. Mater.*, 2022, **34**, 2201262.
11 W. Ren, G. Lin, C. Clarke, J. Zhou and D. Jin, *Adv. Mater.*, 2020, **32**, 1901430.
12 P. Kumar, S. Singh and B. K. Gupta, *Nanoscale*, 2016, **8**, 14297–14340.
13 L. E. MacKenzie and R. Pal, *Nat. Rev. Chem.*, 2021, **5**, 109–124.
14 S. Zhang, W. Yin, Z. Yang, Y. Yang, Z. Li, S. Zhang, B. Zhang, F. Dong, J. Lv and B. Han, *ACS Appl. Mater. Interfaces*, 2021, **13**, 5539–5550.
15 K. Muthamma, D. Sunil and P. Shetty, *Appl. Mater. Today*, 2021, **23**, 101050.
16 X. Zheng, Y. Zhu, Y. Liu, L. Zhou, Z. Xu, C. Feng, C. Zheng, Y. Zheng, J. Bai and K. Yang, *ACS Appl. Mater. Interfaces*, 2021, **13**, 15701–15708.
17 X. Chen, Y. Liu and D. Tu, *Lanthanide-doped luminescent nanomaterials*, Springer, 2016.
18 S. Hao, G. Chen and C. Yang, *Theranostics*, 2013, **3**, 331.
19 G. Rajkumar, V. Ponnusamy, G. V. Kanmani and M. T. Jose, *Ceram. Int.*, 2022, **48**, 10–21.
20 H. Tang, Y. Xu, X. Hu, Q. Hu, T. Chen, W. Jiang, L. Wang and W. Jiang, *Adv. Sci.*, 2021, **8**, 2004118.
21 M. Rakshita, A. A. Sharma, P. P. Pradhan, K. A. K. Durga Prasad, K. Jayanthi and D. Haranath, *Ceram. Int.*, 2023, **49**, 16775–16785.
22 A. Varma, A. S. Mukasyan, A. S. Rogachev and K. V. Manukyan, *Chem. Rev.*, 2016, **116**, 14493–14586.
23 G. Swati, S. Chawla, S. Mishra, B. Rajesh, N. Vijayan, B. Sivaiah, A. Dhar and D. Haranath, *Appl. Surf. Sci.*, 2015, **333**, 178–185.

24 P. Sharma, D. Haranath, H. Chander and S. Singh, *Appl. Surf. Sci.*, 2008, **254**, 4052–4055.
25 R. Rajeswari, C. K. Jayasankar, D. Ramachari and S. Surendra Babu, *Ceram. Int.*, 2013, **39**, 7523–7529.
26 A. Aziz, H. Shaikh, A. Abbas, K. E. Zehra and B. Javed, *Microsc. Res. Tech.*, 2025, **88**, 1599–1614.
27 B. Ko, T. Badloe, Y. Yang, J. Park, J. Kim, H. Jeong, C. Jung and J. Rho, *Nat. Commun.*, 2022, **13**, 6256.
28 M. Shahbazi, H. Jäger, R. Ettelaie, J. Chen, P. A. Kashi and A. Mohammadi, *Adv. Colloid Interface Sci.*, 2024, **333**, 103285.
29 B. Kalaburgi, B. R. Radha Krushna, B. Subramanian, B. Daruka Prasad, K. Manjunatha, S. Yun Wu, A. Shetty and H. Nagabhushana, *Eur. Polym. J.*, 2023, **191**, 112031.
30 L. S. Veiga, O. Garate, G. Giménez, G. Ybarra and L. N. Monsalve, *Nanomaterial-based multifunctional inks for the fabrication of printed biosensors*, 2022.
31 D. Zawar, S. Mishra, M. Rakshita, P. P. Pradhan, K. A. K. Durga Prasad, S. Potu, N. Madathil, J. Pani, N. Kishore Babu and H. Borkar, *Energy Technol.*, 2024, **12**, 2400573.
32 R. Rajeswari, L. Jyothi, C. K. Jayasankar, S. S. Babu, N. Vijayan and D. Haranath, *Sci. Adv. Mater.*, 2013, **5**, 1539–1545.
33 N. C. George, A. J. Pell, G. Dantelle, K. Page, A. Llobet, M. Balasubramanian, G. Pintacuda, B. F. Chmelka and R. Seshadri, *Chem. Mater.*, 2013, **25**, 3979–3995.
34 Y. Zhuo, Y. Niu, F. Wu, J. Li, Y. Wang, Q. Zhang, Y. Teng, X. Xie, H. Dong and Z. Mu, *J. Mater. Chem. C*, 2025, **13**, 10621–10631.
35 A. L. Patterson, *Phys. Rev.*, 1939, **56**, 978.
36 K. S. Nair, P. Abhilash and K. P. Surendran, *ACS Omega*, 2019, **4**, 2577–2583.
37 D. Haranath, S. Sahai, S. Singh, A. G. Joshi, M. Husain and V. Shanker, *J. Mater. Chem.*, 2011, **21**, 9471–9474.
38 Y. Niu, F. Wu, Y. Zhuo, J. Li, Q. Zhang, Y. Teng, X. Xie, H. Dong and Z. Mu, *Ceram. Int.*, 2025, **51**, 30597–30603.
39 E. Nieboer, C. K. Jørgensen, R. D. Peacock, R. Reisfeld and R. D. Peacock, *Rare Earths*, Springer, 1975, pp. 83–122.
40 A. A. Sharma, M. Rakshita, P. P. Pradhan, K. A. K. Durga Prasad, S. Mishra, K. Jayanthi and D. Haranath, *J. Mater. Res.*, 2023, **38**, 2812–2822.
41 W. Ran, H. M. Noh, S. H. Park, B. K. Moon, J. H. Jeong, J. H. Kim and J. Shi, *Sci. Rep.*, 2018, **8**, 1–13.
42 Y. Wu, Y. Nien, Y. Wang and I. Chen, *J. Am. Ceram. Soc.*, 2012, **95**, 1360–1366.
43 P. P. Pradhan, R. Muddamalla, A. A. Sharma, D. P. Kasireddi, A. K, U. K. Khanapuram, R. K. Rajaboina and H. Divi, *ACS Appl. Nano Mater.*, 2023, **6**, 19767–19776.
44 K. A. K. D. Prasad, S. Puranjay, M. Rakshita, A. A. Sharma, P. P. Pradhan, K. U. Kumar, R. R. Kumar and D. Haranath, *J. Fluoresc.*, 2025, **35**(2), 867–875, DOI: **10.1007/s10895-023-03566-9**.
45 K. K. Aitha, D. Dinakar, P. P. Pradhan, K. Yadagiri, K. Suresh, N. Degda, K. V. R. Murthy and D. Haranath, *Can. Metall. Q.*, 2023, 1–9, DOI: **10.1080/00084433.2023.2254128**.
46 V. V. Shinde, S. J. Dhoble and A. N. Yerpude, *Luminescence*, 2024, **39**, e4751.
47 S. Das, S. Som, C.-Y. Yang, S. Chavhan and C.-H. Lu, *Sci. Rep.*, 2016, **6**, 25787.
48 X. Liang, Y. Chen, T. Ouyang, F. Wu, Q. Zhang, Y. Teng, X. Xie, H. Dong and Z. Mu, *J. Photochem. Photobiol., A*, 2026, **470**, 116605.
49 K. A. K. Durga Prasad, M. Rakshita, A. A. Sharma, P. P. Pradhan, K. Uday Kumar, R. Rakesh Kumar and D. Haranath, *J. Appl. Phys.*, 2025, **137**(4), 045102.
50 L. Zhang, R. He and H.-C. Gu, *Appl. Surf. Sci.*, 2006, **253**, 2611–2617.
51 S. Fahmiati, Y. Sampora and J. A. Laksmono, *AIP Conf. Proc.*, 2023, **2902**, 50009.
52 Pushpendra and B. S. Naidu, *Adv. Colloid Interface Sci.*, 2025, **341**, 103480.
53 H. Alidaei-Sharif, M. Babazadeh-Mamaqani, H. Roghani-Mamaqani and M. Salami Kalajahi, *Eur. Polym. J.*, 2023, **197**, 112339.
54 A. I. Kostyukov, N. Y. Kostyukova, A. A. Nashivochnikov, M. I. Rakhmanova and E. A. Suprun, *Opt. Mater.*, 2024, **157**, 116194.
55 R. Mi, Y. Liu, L. Mei, X. Min, M. Fang, X. Wu, Z. Huang and C. Chen, *Chem. Eng. J.*, 2023, **457**, 141377.
56 J. Y. Park, J. W. Chung and H. K. Yang, *Ceram. Int.*, 2019, **45**, 11591–11599.
57 H. M. Abumelha, *Luminescence*, 2021, **36**, 1024–1031.
58 J. V. Rival, P. Mymoona, R. Vinoth, A. M. V. Mohan and E. S. Shibu, *ACS Appl. Mater. Interfaces*, 2021, **13**, 10583–10593.
59 X. Ji, W. Chen, L. Long, F. Huang and J. L. Sessler, *Chem. Sci.*, 2018, **9**, 7746–7752.
60 J. M. Meruga, W. M. Cross, P. Stanley May, Q. Luu, G. A. Crawford and J. J. Kellar, *Nanotechnology*, 2012, **23**(39), 395201, DOI: **10.1088/0957-4484/23/39/395201**.
61 H. Alidaei-Sharif, M. Babazadeh-Mamaqani, M. Mohammadi-Jorjafki, H. Roghani-Mamaqani and M. Salami-Kalajahi, *Macromol. Rapid Commun.*, 2024, **45**, 2400561.
62 J. Kim, H. Kim, H. Kang, W. Kim, Y. Chen, J. Choi, H. Lee and J. Rho, *Nat. Food*, 2024, **5**, 293–300.
63 Q. Jin, H. Li, Y. He, Y. Wang, Y. Chai, Y. Li, X. Huang, H. Li, S. Chen, Y. Li, Z. Wang and M. Wu, *Nano Today*, 2025, **61**, 102621.
64 M. S. Abdelrahman and T. A. Khattab, *Luminescence*, 2024, **39**, e4800.
65 W. Zapka, *Handbook of industrial inkjet printing: a full system approach*, John Wiley & Sons, 2018, vol. 1.
66 W. Shi, J. Chen, J. Kong, Z. Ma, J. Gao, J. Guo, Z. Hu, Q. Lv, B. Deng and W. Chen, *J. Alloys Compd.*, 2022, **914**, 165134.
67 K. N. Narasimhamurthy, B. D. Prasad, D. R. Lavanya, D. Kavyashree, G. P. Darshan, S. C. Sharma, H. B. Premkumar, K. S. Kiran and H. Nagabhushana, *Colloids Surf., A*, 2022, **634**, 127770.
68 V. Sangwan, M. Jayasimhadri and D. Haranath, *J. Phys. D: Appl. Phys.*, 2024, **57**, 195301.
69 C. Zhuo, S. Zhao, X. Huang, Y. Jiang, J. Li and D.-Y. Fu, *J. Mol. Liq.*, 2023, **376**, 121442.
70 J. Huang, Q. Guo, R. Zhu, Y. Liu, F. Xu and X. Zhang, *Int. J. Biol. Macromol.*, 2021, **189**, 635–640.

